This article has been accepted for publication in a future issue of this journal, but has not been fully edited. Content may change prior to final publication. Citation information: DOI 10.1109/JLT.2019.2923783, Journal of Lightwave Technology

Iterative Block Decision Feedback Equalization for IM/DD-Based OCDM to Compensate Chromatic-Dispersion-Induced Power Fading

Xing Ouyang, *Member, IEEE*, Giuseppe Talli, Mark Power and Paul D. Townsend

***Abstract*—Orthogonal chirp-division multiplexing (OCDM) has recently been proposed as an attractive modulation technique for high-speed fiber-optic systems in virtue of its resilience against system impairments. In this paper, we propose an iterative block (IB) decision feedback equalization (DFE) algorithm for the intensity-modulation and direct-detection (IM/DD) based OCDM system to effectively mitigate the chromatic-dispersion (CD)-induced power fading in the fiber. An efficient algorithm is derived to simplify the IB-DFE at the receiver. Analysis is provided to show that the fading effect is compensated by recovering the noisy signals in the vicinity of frequency notches. Simulations were carried out to study the performance of the proposed system. The results show that the proposed system with IB-DFE is able to compensate severe fading effects and improves the bit-error rate (BER) by several orders of magnitude. An experiment was implemented to realize 30.3-Gbit/s IM/DD-OCDM signal over 50-km fiber, in which power fading due to CD over 20 dB was observed. The experiment results show that the proposed system further reduced the required OSNR by 8 dB to achieve a BER of 3×10^{-5}.**

***Index Terms*—Discrete Fresnel transform (DFnT), orthogonal chirp-division multiplexing (OCDM), iterative block decision feedback equalization (IB-DFE), chromatic-dispersion induced power fading, intensity modulation, direct detection.**

I. Introduction

During recent decades, advances in ultra-high-speed digital signal processing (DSP) technology has substantially boosted the capacity of fiber-optic systems to enable continuing support for the ever-increasing demand for high-speed Internet and data services [1-3]. Enabled by advanced DSP technology, orthogonal chirp-division multiplexing (OCDM) has been recently proposed and demonstrated as an attractive modulation technique for high-speed digital coherent lightwave systems [4-6]. In the coherent optical (CO) OCDM system, a large bank of linearly frequency-modulated waveforms, so-called chirps, are synthesized for high-speed information modulation [4]. In contrast to conventional chirp spread spectrum (CSS), the chirps in OCDM are mutually orthogonal in the sense of the Nyquist signaling, achieving the maximum spectral efficiency without any interference among them [6]. Moreover, by virtue of the spread-spectrum feature of the chirped waveforms, the OCDM signal is capable of effectively mitigating impairments, such as, interference and clock leakage in a fiber-optic system. As a result, OCDM exhibits superior performance in comparison with other modulation techniques, such as, orthogonal frequency-division multiplexing (OFDM) [4-9].

Considering the advantages of OCDM, it is highly desirable that the scheme is adapted for optical intensity-modulated and direct-detection (IM/DD) systems, in which performance degrading impairments can be much more difficult to control in contrast to coherent systems. One example is the chromatic-dispersion-induced power fading that arises as the dispersive optical frequencies beat at the photodiodes [10]. The chromatic dispersion (CD)-induced fading impairs the signal at high frequencies, and increases quadratically with signal bandwidth. Nonetheless, due to simplicity, low cost, and small footprint, IM/DD systems are the preferred solution for short-reach applications, such as, next-generation passive optical networks (PON) and datacenter interconnects [11-13]. In this work, we show how the impairment mitigation characteristics of OCDM make it an attractive candidate for future high-speed, short-reach IM/DD-based systems by counteracting these impairments [14].

In this paper, we present a double-sideband (DSB) modulated OCDM for realizing IM/DD systems, which exhibits superior impairment resilience compared to OFDM system. An iterative block decision feedback equalization (IB-DFE) is proposed to further improve the performance of IM/DD-OCDM by mitigating the CD-induced power fading. In the proposed scheme, the IB-DFE compensates non-ideal all-pass-filtering effects, such as CD-induced fading, by recovering the signals in the vicinity of frequency notches. In addition, by utilizing the eigen-decomposition property of the discrete Fresnel transform (DFnT), a simplified IB-DFE algorithm is derived to implement the proposed system efficiently.

Simulations were carried out to confirm the feasibility and advantages of the proposed scheme, and extended numerical results and detailed analysis are provided here to our previous work in [15]. It is shown that the proposed IM/DD-OCDM with IB-DFE effectively alleviates degradation, such as, CD-induced

This work is supported by Science Foundation Ireland (SFI) under the grants 12/IA/1270 and 12/RC/2276.

The authors are with Photonics Systems Group, Tyndall National Institute, University College Cork, Lee Maltings complex, Dyke Parade, cork city center, CORK, T12 R5CP Ireland. (E-mail: xing.ouyang@tyndall.ie, giuseppe.talli@tyndall.ie, paul.townsend@tyndall.ie).

This article has been accepted for publication in a future issue of this journal, but has not been fully edited. Content may change prior to final publication. Citation information: DOI 10.1109/JLT.2019.2923783, Journal of Lightwave Technology

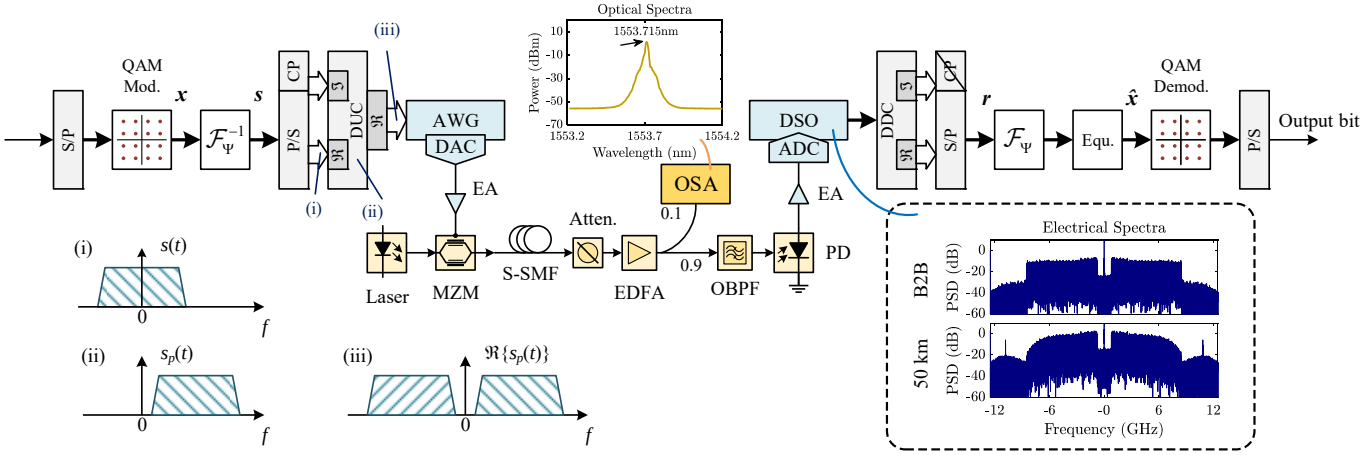

Fig. 1. System setup of the IM/DD-OCDM system based on digital up-conversion. The insets illustrate the spectra of (i) the equivalent complex-baseband OCDM signals, (ii) the up-converted passband signals, and (iii) the real part (DSB) of the signals. Abbreviations: P/S: Parallel-to-Serial; S/P: Serial-to-Parallel; DUC: Digital Up-Conversion; DDC: Digital Down-Conversion; AWG: Arbitrary Waveform Generator; DSO: Digital Sampling Oscilloscope; DAC/ADC: Digital-to-Analog/Analog-to-Digital Convertor; MZM: Mach-Zehnder Modulator; EDFA: Erbium-Doped Fiber Amplifier; PD: Photodiode.

fading. As a result, the bit-error rate (BER) performance can be improved by several orders of magnitude after fiber transmission with severe fading effect. Moreover, experiments were implemented to demonstrate the IM/DD-OCDM with IB-DFE for the first time in which a 30.8-Gbit/s OCDM signal was successfully transmitted over a 50-km standard single-mode fiber (S-SMF). It is shown that the proposed system outperforms the OFDM system significantly even without IB-DFE. If the IB-DFE is applied, the performance is significantly improved. For example, the BER is reduced from 3×10^{-5} to 4×10^{-7}, 2×10^{-8} and 6×10^{-9} at an optical signal-to-noise ratio (OSNR) = 46 dB with 1, 2 and 4 iterations, respectively.

This paper is organized as follows. In Section II, the system model of the proposed IM/DD-OCDM system with the IB-DFE is presented, and the simplified algorithm is derived. The power fading effect in IM/DD systems is discussed to show how the proposed system compensates the fading effect in the frequency domain. Simulation and experiment are provided in Section III and IV, respectively, to validate the feasibility and advantages of the proposed scheme. Discussions are provided in Section V, and Section VI finally concludes this paper.

II. Proposed IM/DD-OCDM System with IB-DFE

An OCDM signal is essentially a bank of orthogonal chirps, each of which is individually modulated by an information symbol. The complex-baseband OCDM signal, $s(n)$, can be digitally synthesized by using the inverse DFnT (IDFnT) with fast algorithms [16], as

$$\begin{aligned} s(n) &= \mathcal{F}_\Psi^{-1}\{x(k)\}(n) \\ &= \frac{1}{\sqrt{N}} e^{j\frac{\pi}{4}} \sum_{k=0}^{N-1} x(k) \times \begin{cases} e^{-j\frac{\pi}{N}(n-k)^2} & N \equiv 0 \pmod 2 \\ e^{-j\frac{\pi}{N}\left(n-k+\frac{1}{2}\right)^2} & N \equiv 1 \pmod 2 \end{cases} \end{aligned} \tag{1}$$

where $\mathcal{F}_\Psi^{-1}$ is the IDFnT operator, and $x(k)$ is the symbol modulating the k-th chirp. In Eq. (1), the Fresnel transform, similar to Fourier transform, is a trigonometric transformation, but with quadratic phase [17]. This discrete version of Fresnel transform, which has attractive properties for signal processing, is first derived in [16]. Based on its orthogonality, the DFnT can multiplex modulated chirps without any interference. Fast algorithm is also shown in [16] to calculate the DFnT with the same order of complexity as the fast Fourier transform, and the generation of OCDM signal can be as computationally efficient as the OFDM signal. Based on the circular convolution property of the DFnT, cyclic prefixes (CP) can be inserted between OCDM symbols as the guard interval (GI) to avoid inter-symbol interference (ISI) during transmission. At the receiver, as shown in Fig. 1, inverse operations are performed to recover the transmitted information [5].

A. DSB-Modulated OCDM for IM/DD Systems

In the conventional OCDM system, the signals in Eq. (1) are complex-valued, which cannot be directly applied for intensity modulation, for example, by driving a Mach-Zehnder modulator (MZM). To overcome this hurdle, an IM/DD-OCDM system was proposed based on digital up-conversion (DUC) [14]. In the proposed IM/DD-OCDM, as shown in Fig. 1, the baseband OCDM signal is first up-converted by a digital carrier, with a frequency f_p, up to a passband. By discarding the imaginary part, the real part of the signal is a DSB-modulated OCDM signal, which is given by

$$\begin{aligned} \Re\{s_p(t)\} &= \Re\left\{e^{j2\pi f_p t} s(t)\right\} \\ &= s_I(t)\cdot\cos 2\pi f_p t - s_Q(t)\cdot\sin 2\pi f_p t\,, \end{aligned} \tag{2}$$

where $s_I(t)$ and $s_Q(t)$ are the inphase and quadrature components of $s(t)$, respectively. The insets in Fig. 1 show the signal spectra of the DUC process. As the output of the DUC is a real-valued signal, it can be directly used for intensity modulation.

At the receiver, digital down-conversion (DDC) is performed to convert the signal back to the baseband, and a conventional OCDM receiver can be employed to recover the signal. The received signal after removing GI is given by

This article has been accepted for publication in a future issue of this journal, but has not been fully edited. Content may change prior to final publication. Citation information: DOI 10.1109/JLT.2019.2923783, Journal of Lightwave Technology

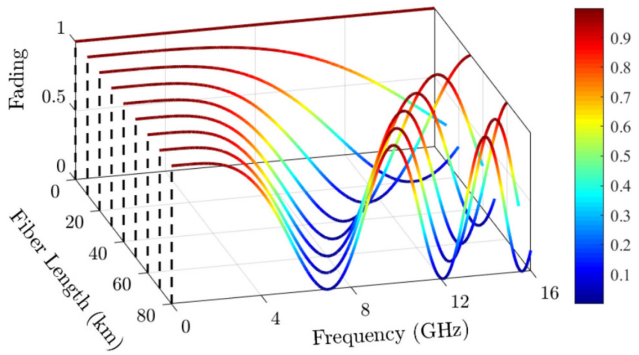

Fig. 2. Chromatic-dispersion-induced power fading effect in an IM/DD system with standard single-mode fiber at 1550 nm.

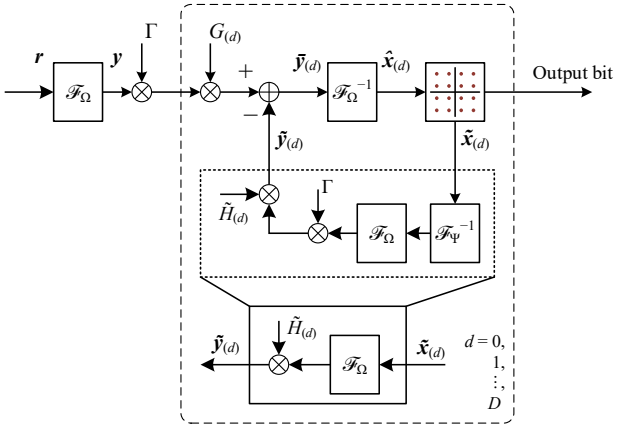

Fig. 3. Block diagram of the proposed IB-DFE receiver for the IM/DD-OCDM systems.

$$r(n) = h(n) \otimes s(n) + v(n), \tag{3}$$

where $\otimes$ is the circular convolution, $h(n)$ and $v(n)$ are the channel impulse response (CIR) and the additive noise, respectively.

B. Chromatic-Dispersion-Induced Fading in IM/DD-OCDM

In Eq. (3), $h(n)$ can characterize not only the CD effects, but also other linear effects arising from electrical or optical filters and amplifiers, for example. In IM/DD systems, chromatic dispersion imposes a severe fading effect on the received signals. As shown in Fig. 2, it imposes power notches at high frequencies, which severely limit the system performance. The transfer function of CD in IM/DD systems [18] is given by

$$H_{\mathrm{CD}}(f) \propto \cos\left(2\pi^2 \beta_2 f^2 z\right), \tag{4}$$

where f denotes the frequency, β_2 is the group velocity dispersion (GVD) parameter, and z the length of fiber.

In the simplified receiver scheme, the received signal in Eq. (3) is transformed to the frequency domain by a discrete Fourier transform (DFT), as

$$\begin{aligned} y(m) &= \mathcal{F}_\Omega\{r(n)\}(m) \\ &= H(m) \times \mathcal{F}_\Omega\{s(n)\}(m) + v_\Omega(m), \end{aligned} \tag{5}$$

where $\mathcal{F}_\Omega$ is the discrete Fourier transform (DFT) operator, and $H(m)$ is the channel frequency response (CFR). By utilizing the eigen-decomposition property of the Fresnel transform,

$$\mathcal{F}_\Omega\left\{\mathcal{F}_\Psi^{-1}\{x(k)\}\right\}(m) = \Gamma^*(m) \times \mathcal{F}_\Omega\{x(k)\}(m), \tag{6}$$

Eq. (5) can further arrive at

$$y(m) = H(m)\Gamma^*(m) \times \mathcal{F}_\Omega\{x(k)\}(m) + v_\Omega(m), \tag{7}$$

where $\Gamma(m)$ is the eigen-value of DFnT w.r.t DFT. Based on Eq. (7), the information symbols can be recovered by compensating the CFR $H(m)$ and phase rotation $\Gamma^*(m)$, followed by an inverse DFT (IDFT). As shown in Fig. 1, the estimated symbols, $\hat{x}(m)$, can be used to recover the information bits.

C. IB-DFE algorithm for the IM/DD-OCDM

In order to compensate the CD-induced power fading effect, in this paper, the IB-DFE algorithm [19-21] is proposed for the IM/DD-OCDM system. An efficient algorithm is proposed to simplify the IB-DFE receiver by utilizing the eigen-decomposition property of the DFnT, as shown in Fig. 3. In principle, the feedback signal should be re-modulated and distorted by the residual ISI. By using the eigen-decomposition property of DFnT in Eq. (7), the feedback signal can be simplified as

$$\begin{aligned} \tilde{y}_{(d)}(m) &= \tilde{H}_{(d)}(m)\Gamma(m) \times \mathcal{F}_\Omega\left\{\mathcal{F}_\Psi^{-1}\left\{\tilde{x}_{(d)}(k)\right\}\right\}(m) \\ &= \tilde{H}_{(d)}(m) \times \mathcal{F}_\Omega\left\{\tilde{x}_{(d)}(k)\right\}(m), \end{aligned} \tag{8}$$

where $\tilde{x}_{(d)}(k)$ is the estimate of the transmitted symbol based on the decision on $\hat{x_{(d)}}(k)$, and $\tilde{H}_{(d)}(m)$ is the residual ISI in the frequency domain for the d-th iteration. It should be noted that, in the initial stage, namely, $d = 0$, there is no feedback by assuming $\tilde{y}_{(d)}(k) = 0$. In the second equation of Eq. (8), only one DFT and residual ISI distortion are required by saving one IDFnT in the first. The output of the IB-DFE is thus

$$\begin{aligned} \overline{y}_{(d)}(m) &= G_{(d)}(m)\Gamma(m) \times y(m) - \tilde{y}_{(d)}(m) \\ &= G_{(d)}(m)H(m) \times \mathcal{F}_\Omega\{x(k)\}(m) \\ &\quad - \tilde{H}_{(d)}(m) \times \mathcal{F}_\Omega\left\{\tilde{x}_{(d)}(k)\right\}(m). \end{aligned} \tag{9}$$

where $G_{(d)}(m)$ are the coefficients of the feedforward equalizer.

In the ideal case that the estimate is perfect, i.e., $\tilde{x}(d) = x(k)$, the matched filter is optimal to completely compensate the fading, and the feedforward and feedback equalizers' taps are

$$G_{(d)}(m) = H^*(m), \tag{10}$$

and

This article has been accepted for publication in a future issue of this journal, but has not been fully edited. Content may change prior to final publication. Citation information: DOI 10.1109/JLT.2019.2923783, Journal of Lightwave Technology

$$\tilde{H}_{(d)}(m) = \langle H(m) \rangle - |H(m)|^2 , \tag{11}$$

respectively. In (10), we can see that the feedforward equalizer is essentially a matched-filter, which maximizes the received SNR. On the right-hand-side of (11), the first term is the mean value of CFR and the second is the matched CFR as $|H(m)|^2 = H^*(m)H(m)$. Thus, the feedback taps in Eq. (11) are interference terms in the frequency domain. Plugging both (10) and (11) into Eq. (9), one can obtain

$$\bar{y}_{(d)}(m) = \langle H(m) \rangle \times \mathcal{F}_{\Omega}\{x(k)\}(m). \tag{12}$$

This means that if the feedback symbols are correctly estimated, a matched-filter yields an IB-DFE output which is exactly equal to the transmitted signal with no fading effect. In other words, the entire system is equivalent to an all-pass filter without any distortion from the fading effect. In practice, however, the symbols cannot be perfectly estimated due to noise and severe distortion, and the errors in the feedback loop will limit the performance. Therefore, sophisticated design of the feedforward and feedback equalizers should be considered to minimize the decision errors [22].

III. Simulations

In this section, numerical simulation was carried out to study the proposed IM/DD-OCDM system based on IB-DFE. The following subsections provide the simulation setup and results, respectively.

A. Simulation Setup

The system setup is shown in Fig. 1. At the transmitter, there were 512 chirps modulated in quadrature amplitude modulation (QAM). The baseband OCDM signal was generated with an oversampling of 4. The DSB-modulated OCDM signal was obtained by DUC, and the signal was then converted to an analog signal by a digital-to-analog converter (DAC) operating at 32 GSa/s to drive a MZM, which was assumed to be operated within its linear region. As a result, the complex-baseband signal had an 8-GHz bandwidth. In the DUC, the up-conversion frequency was 4.125 GHz, and the DSB signal at the output of the DUC was 8.125 GHz. The laser was operated at 1553 nm, and standard SMF (S-SMF) was adopted, with a dispersion of 16 ps/(nm·km) and attenuation of 0.2 dB/km.

At the receiver, an erbium-doped fiber amplifier (EDFA) was used to compensate attenuation with an optical band-pass filter (OBPF) to remove the out-of-band amplified spontaneous emission (ASE) noise. The signal was detected by a photodiode (PD) and then transformed to the digital domain by an analog-to-digital converter (ADC). In the simulation, the received optical signal-to-noise ratio (OSNR) was measured with a resolution of 0.1 nm. The DDC converted the signal back to the baseband for recovery. The signal was fed to the IB-FDE block as shown in Fig. 3, and was iteratively detected by updating the taps of the FFE and DFE. For comparison, discrete multi-tone (DMT) based OFDM was adopted. The DMT-OFDM had 2048 subcarriers. The first 8 subcarriers were unmodulated to avoid AC coupling, and the following 512 subcarriers were modulated with payload. The CP overhead of both systems was 1/64, and

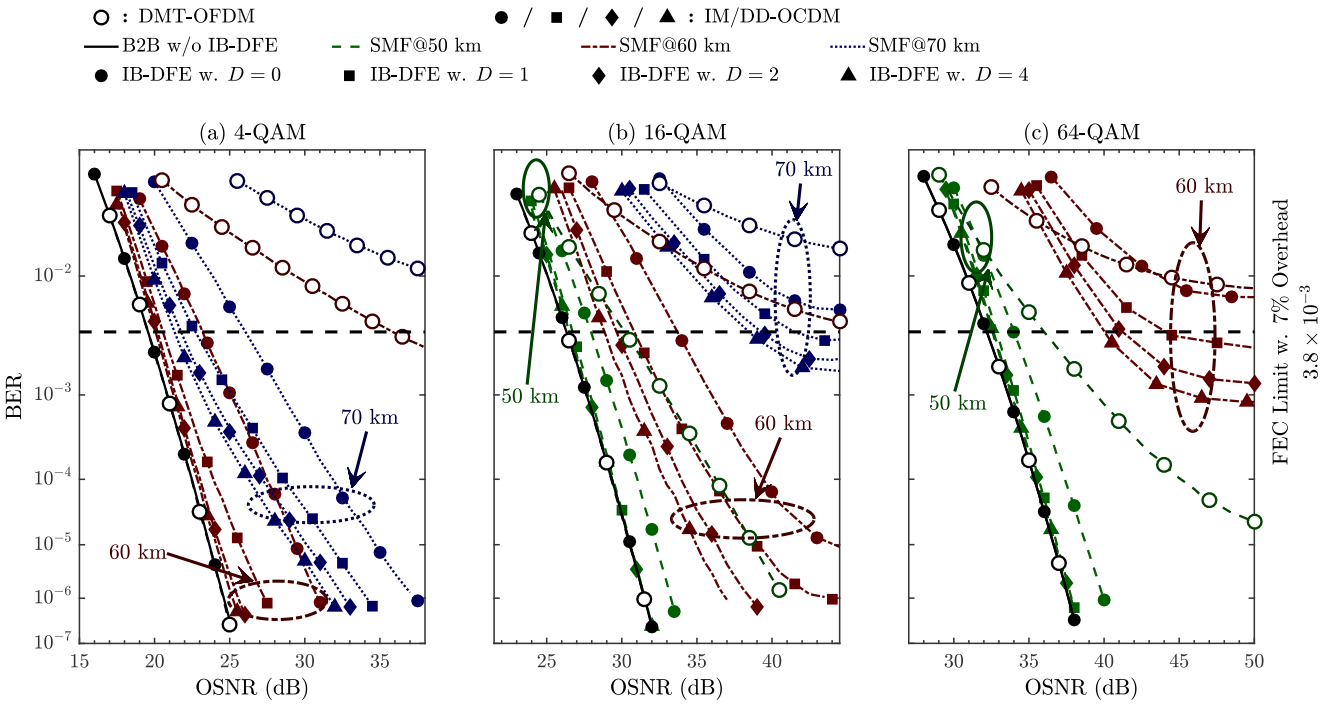

Fig. 4. BER versus OSNR performance of DMT-OFDM and IM/DD-OCDM systems with various modulation formats (a) 4-QAM, (b) 16-QAM, and (c) 64-QAM. Curves with hollow circles (○) denotes OFDM system at different distances. Curves with solid marks (●/■/◆/▲) denotes OCDM system with IB-DFE of different iterations (D = 0, 1, 2, and 4 respectively).

This article has been accepted for publication in a future issue of this journal, but has not been fully edited. Content may change prior to final publication. Citation information: DOI 10.1109/JLT.2019.2923783, Journal of Lightwave Technology

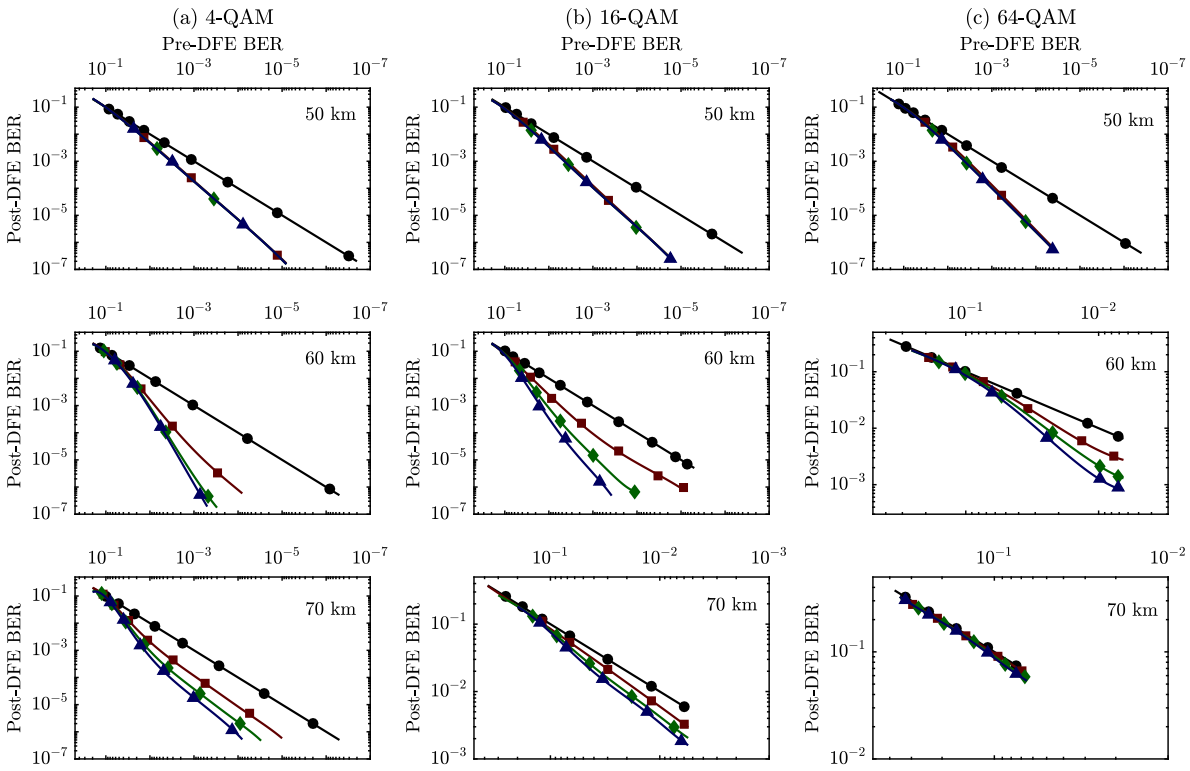

Fig. 5. The Post-DFE BER improvement of IB-DFE receiver for (a) 4-QAM, (b) 16-QAM, and (c) 64-QAM. Markers {●, ■, ♦, and ▲} denote IB-DFE with iterations D = {0, 1, 2, and 4}.

thus was 32 points per symbol. To generate the real-valued signal, the negative subcarriers were the complex conjugate of the positive symmetries. By doing so, the DMT-OFDM had the same data rate as that of the OCDM for a fair comparison.

B. Simulation Results

In this subsection, the performance of the proposed IM/DD-OCDM signal with different modulation levels is studied. The data rates excluding CP are 16, 32, and 48 Gb/s for 4-, 16-, and 64-QAM, respectively. Fig. 4 shows the bit-error rate (BER) performance against received OSNR. It can be seen in Fig. 4 (a) that 4-QAM can support transmission up to 70 km with about 7-dB OSNR penalty compared to the back-to-back (B2B) case at a BER = 10^{-3}. Degradation in BER becomes more severe for higher-level formats. For example, error floors occur in the 16-QAM case at 70 km and 64-QAM cannot support a transmission beyond 60 km without IB-DFE.

These results agree well with the analytical CD-induced fading effect shown in Fig. 2, where the first frequency notch due to the CD occurs at ~8-GHz at 60 km. If the IB-DFE is applied, substantial improvement can be observed in all cases. In Fig. 4 (a), for example, the BER of 4-QAM signals at 60 km is improved by two orders of magnitude from 10^{-3} to 10^{-5} at OSNR = 29 dB with number of iterations D = 4. For 16-QAM at 60 km, the BER is improved by almost three orders of magnitude from 10^{-3} to 10^{-6} with D = 4 at OSNR = 37 dB. At 70 km, the improvement is limited due to the decision errors in the feedback loop as the fading has already severely distorted the signal. Nonetheless, the IB-DFE improves the BER from ~6×10^{-3} to 2×10^{-3}, below the FEC limit of 3.8×10^{-3} with 7% overhead.

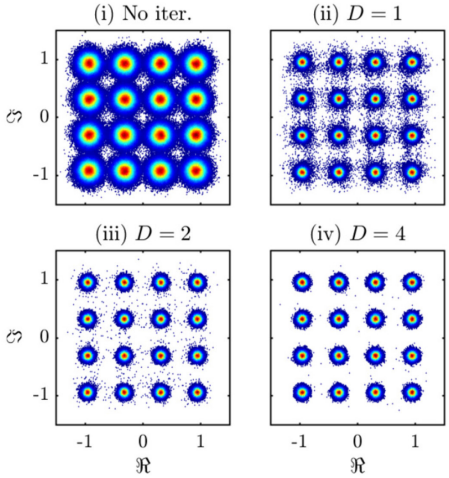

Fig. 6. Constellation diagrams of the received 16-QAM signals, at a received OSNR = 33 dB after 60-km transmission, with numbers of iterations D = 0 (no iteration), 1, 2, 4 from (i) to (iv).

Fig. 4 (c) shows that 64-QAM is more sensitive to the distortions, and it does not support a distance beyond 60 km. Still, the BER at 60 km is improved from 7×10^{-3} to 8×10^{-4}, well below the FEC limit.

For comparison, the performance of the DMT based OFDM is provided. It can be seen that the OFDM has the same performance as the OCDM without fiber transmission as there is no fading effect nor other severe impairments. As the transmission distance increases, the degradation in the OFDM is more obvious than the OCDM without IB-DFE at the same transmission distance. For example, in the case of 16-QAM at 50 km, OFDM

This article has been accepted for publication in a future issue of this journal, but has not been fully edited. Content may change prior to final publication. Citation information: DOI 10.1109/JLT.2019.2923783, Journal of Lightwave Technology

requires an extra 8-dB OSNR to achieve a BER = 10^{-6} compared to the OCDM without IB-DFE. If the distance increases to 60 km, OFDM has a BER performance worse than 4×10^{-3} even if the received OSNR is over 40 dB, while OCDM can attain a BER around 1×10^{-5} without IB-DFE. If IB-DFE is adopted, the advantage of OCDM is even more obvious with about 9-dB OSNR improvement for OCDM with 4 iterations.

In Fig. 5, the Pre-DFE versus Post-DFE BER performance is shown to provide a deeper insight into the mechanism of the IB-DFE. It can be seen that at a distance of 50 km, the degradation in all cases can be fully compensated with $D = 1$ iteration since no severe notch exists within the system bandwidth. At 60 km, as the frequency nulls are close to the signal bandwidth, the IB-DFE algorithm can improve the BER by iterations up to $D = 4$. The improvement is obvious if the Pre-DFE BER is acceptable, we say below ~1×10^{-2}. However, if the Pre-DFE BER is worse, for example, at a distance of 70 km, only marginal improvement is observed in the case of 16-QAM, and almost no improvement at all in the case of 64-QAM.

In Fig. 6, the constellation diagrams of the received 16-QAM signal at an OSNR = 30 dB and 60 km are shown. It can be seen that, as the number of iterations, D, increases, the interference due to CD-induced power fading can be significantly mitigated. The constellations become much clearer and more clustered. It should be noted that in Fig. 6 (iv), even if the constellations are clustered with an iteration number of $D = 4$, there are still scattered errors in the diagram. The errors are from the decision errors in the feedback loop, and they are more likely to affect adjacent symbols.

IV. Experiments

In this section, experiments were also implemented to further investigate the feasibility and performance of the proposed system. The experiment setup and results along with related discussions are provided in the following subsections.

A. Experiment Setup

In the experiment, the system setup can be also shown by Fig. 1. At the transmitter, the signal was generated offline based on the model in Section II, and downloaded to an arbitrary waveform generator (AWG), which was operated at a sampling rate of 25 GSa/s. The laser centered at 1553.75 nm and the Mach-Zehnder modulator (MZM) had a V_π of ~5 V. The signal at the output of the AWG was amplified to a V_{pp} of ~3.5V to drive the MZM at the quadrature point. A spool of standard single mode fiber (S-SMF) with a length of 50 km was adopted.

At the receiver, a variable optical attenuator was placed at the output of the fiber to control the optical power into the erbium-doped fiber amplifier (EDFA). Following the EDFA, there was a 90:10 splitter. The 10% port was connected to an optical spectral analyzer (OSA) to monitor the received OSNR with 0.1-nm resolution. The 90% port was connected to a 0.6-nm optical filter to remove the out-of-band amplified spontaneous emission (ASE) noise. An optical power controller was placed at the output of the optical filter to maintain the input power to the PD at 9 dBm. Following the PD, an electrical amplifier (EA) amplified the signal and a 100-GSa/s digital sampling oscilloscope (DSO) captured the signal for offline processing.

Similar to the simulation, both the DMT-OFDM and the proposed IM/DD-OCDM systems were implemented for comparison. In the proposed IM/DD-OCDM, both the DUC and DDC were realized in the frequency domain by utilizing the Fourier transform. As we employed only a 50-km S-SMF, the effect of the CD-induced fading was studied by varying the signal bandwidth rather than varying the fiber length. In the experiment, the number of chirps in OCDM varied from 540 to 630, and we fixed the block length to 2048. The bandwidths of the complex-baseband OCDM signal accordingly varied from 6.59 to 7.69 GHz. The up-conversion frequency is 4.63 GHz, and resulting bandwidth of the up-converted signal was 8.5 GHz. For a fair comparison, in the DMT-OFDM, there were 2048 subcarriers, of which 540 to 630 were modulated with payload and of which the first 64 subcarriers were zero. In the DMT-OFDM, to avoid AC coupling, the first 64 subcarriers were set to be zeros. The negative subcarriers were the complex conjugate of the symmetric subcarrier in the positive frequency to obtain real-valued DMT signals. In both systems, CP was 32-point in length, and 16-QAM was adopted. As a result, both systems had the same effective bandwidth and also the same data rate, which was 30.3 Gbit/s including the GI overhead for the 7.69-GHz setup.

B. Channel State Information Characterization

To optimize the experiments and show how the proposed algorithm compensates the fading effect, we measured the channel state information (CSI), which is shown in Fig. 7, in terms of (a) the channel impulse response and (b) the channel frequency response (CFR) of the whole system, and (c) the transfer function of the CD-induced fading in the fiber. The CSI was obtained by using channel estimation based on the intra-symbol frequency-domain averaging algorithm [23]. It should be noted

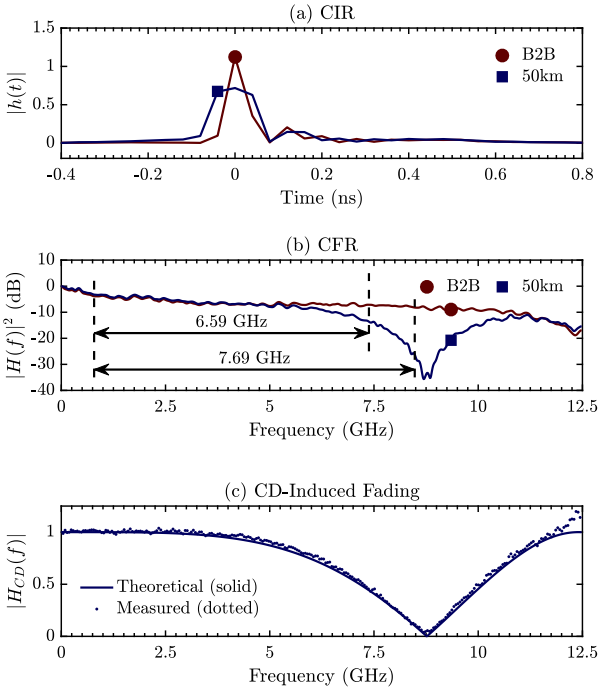

Fig. 7. Measured channel state information (CSI) based on channel estimation: (a) channel impulse response (CIR), (b) channel frequency response (CFR), and (c) the transfer function of the CD-induced fading in the fiber link.

This article has been accepted for publication in a future issue of this journal, but has not been fully edited. Content may change prior to final publication. Citation information: DOI 10.1109/JLT.2019.2923783, Journal of Lightwave Technology

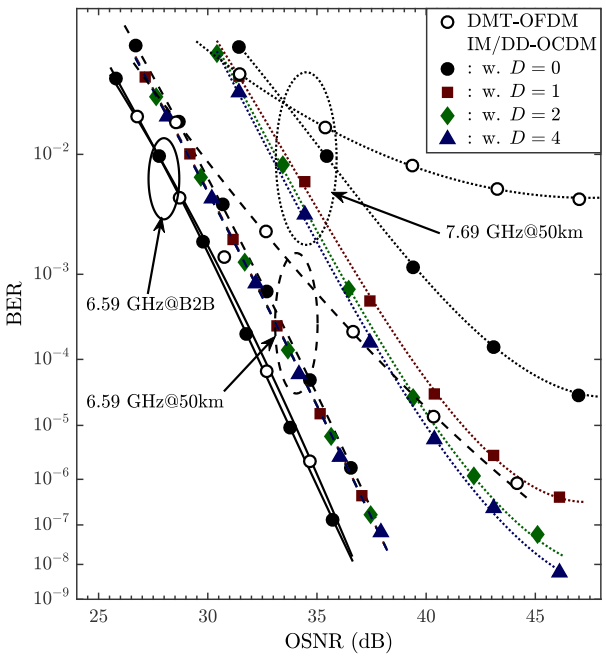

Fig. 8. Measured BER versus OSNR performance of the DMT-OFDM and the proposed IM/DD-OCDM systems with a data rate at 30.3 Gbit/s at 50 km.

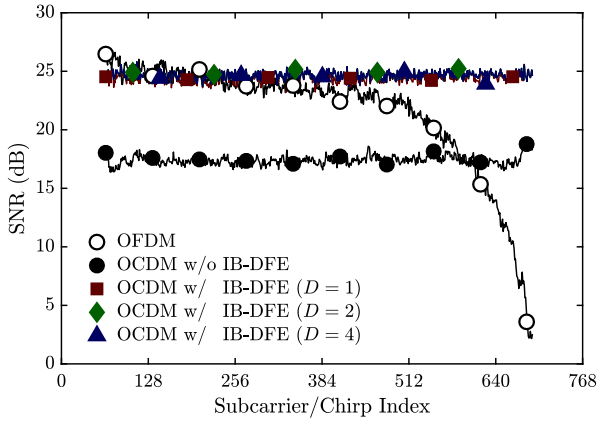

Fig. 9. Measured SNR of the subcarriers in DMT-OFDM and the chirps in the proposed IM/DD-OCDM with and without IB-DFE at an OSNR = 40 dB and 30.3 Gbit/s after 50 km.

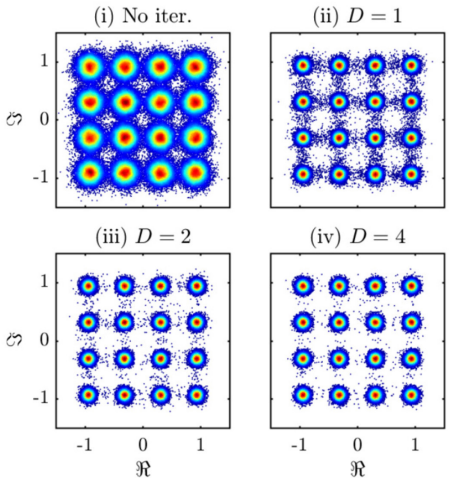

Fig. 10. Measured constellation diagrams of the received 16-QAM signal, at a received OSNR = 36 dB after 50-km transmission, with numbers of iterations $D = 0$ (no iteration), 1, 2, 4 from (i) to (iv), respectively.

that other channel estimation algorithm can also be applied for the proposed system, especially the unbiased channel estimator proposed for OCDM in [24, 25]. In Fig. 7 (a), the pulse broadening of the system is about 0.25 ns at B2B, and the pulse broadening due to fiber transmission is ~0.05 ns. The result fits the analytical dispersion of a 50-km S-SMF with a dispersion parameter of 16 ps/(nm·km) at 1553 nm.

In Fig. 7 (b), the transfer function of the system is plotted. In the B2B case, the CFR function gradually decreases to −7dB at 7.69 GHz, which is mainly caused by the electronic components. After 50 km transmission, a severe fading effect occurs, and the CFR function decreases to −27 dB at 8.5 GHz. Because of CD, a frequency null at 8.8 GHz is observed, which conforms to the analytical result in Fig. 2. To illustrate the CD-induced fading effect, Fig. 7 (c) provides the transfer function of the fiber. It can be seen that the measured transfer function (dotted line) fits the analytical result (solid line) well, and a frequency null due to CD occurs at 8.8 GHz.

According to the measured CSI, in the experiments, the two setups are chosen to study the capability of the proposed system on compensating the fading effect. In the first setup, the signal has a bandwidth of 6.59 GHz, which is far away from the notch. In this case, there is no severe fading observed within the signal bandwidth. In the second setup with 7.69-GHz bandwidth, as the signal is close to the frequency notch, as shown in Fig. 7 (b), it can be expected that the proposed IB-DFE algorithm can effectively mitigate the degradation due to the fading effect.

C. *BER Performance of Open-Loop System*

Fig. 8 shows the BER performance of both DMT-OFDM and the proposed IM/DD-OCDM systems. The performance trend is similar to the simulation in Section III. In the B2B case, both systems have almost the same performance. After 50-km fiber transmission, the BER curves of the OCDM signals with 6.59-GHz bandwidth have steeper slopes than that of OFDM. The OCDM requires 7 dB less OSNR than OFDM to attain BER = 10^{-6}. The improvement of OCDM over OFDM is obvious, while the improvement of the OCDM with IB-DFE is minor compared to that without IB-DFE. This implies that the OCDM signal has better resilience to the impairments than the OFDM signal, yet the IB-DFE contributes only a minor improvement as the fading effect in this case is not so severe.

To investigate the performance of IB-DFE, the signal bandwidth is increased to 7.69 GHz, approaching the frequency notch. It can be seen that significant improvement is achieved by the OCDM with IB-DFE. At OSNR = 46 dB, the OCDM without IB-DFE has a BER ≈ 3×10^{-5}. If IB-DFE is applied, the BER is improved to ~4×10^{-7}, 2×10^{-8} and 6×10^{-9} with 1, 2 and 4 iterations, respectively. To achieve a BER of 3×10^{-5}, the IB-DFE with 4 iterations reduces the required OSNR from 46 dB to 39 dB, a 7-dB improvement. In contrast, in the DMT-OFDM, an error floor occurs at 5×10^{-3}, which is above the FEC limit at 3.8×10^{-3}.

To show how the proposed algorithm works, the SNR of the subcarriers in OFDM and the chirps in OCDM were measured

This article has been accepted for publication in a future issue of this journal, but has not been fully edited. Content may change prior to final publication. Citation information: DOI 10.1109/JLT.2019.2923783, Journal of Lightwave Technology

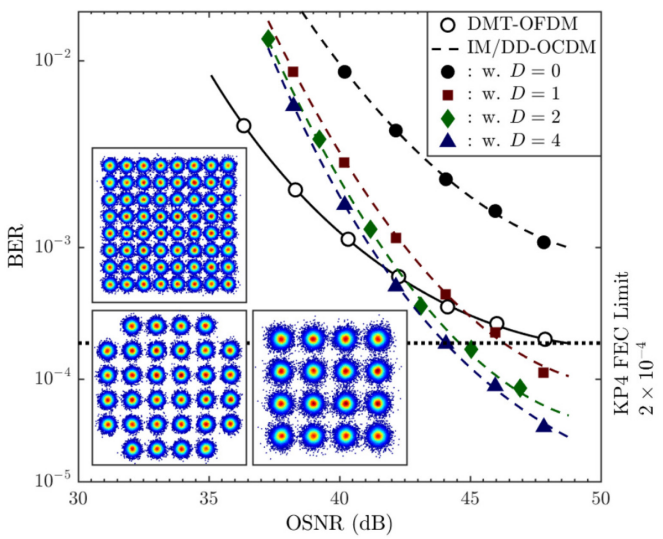

Fig. 11. Measured BER versus OSNR of the adaptive modulated DMT-OFDM and the proposed IM/DD-OCDM systems with 32-QAM at a data rate at 37.9 Gbit/s at 50 km. The insets are received constellation diagrams of the adaptive modulation DMT signal at an OSNR = 40 dB.

at a received OSNR = 40 dB, as shown in Fig. 9. In OFDM, the subcarriers in the low frequency region achieve better performance than the chirps in the OCDM without IB-DFE. However, as the frequency increases, the SNR of the subcarriers degrades dramatically, and SNR as low as 3 dB is observed. The noisy subcarriers impaired by the CD-induced power fading in the high frequency region mainly limit the performance of the OFDM. On the other hand, for the OCDM without IB-DFE, the chirps are insensitive to the fading effect, and thus have almost constant SNR. This explains why the OCDM signal has better performance than the OFDM signal even without IB-DFE. If the IB-DFE algorithm is applied, the performance of the OCDM signal improves and attains almost the same SNR as the OFDM signal in the low frequency region. This is because the signal in the high frequency region is compensated by IB-DFE and the overall signal quality is optimized to an SNR in terms of the matched filter, as analytically shown in Section II.

It should be noted that with IB-DFE, the chirps have almost the same SNR as long as $D \geq 1$. However, this does not mean that a single iteration of IB-DFE corrects all the errors. The performance of the chirps depends on the decision errors in the feedback loop, namely $\tilde{x}_{(d)}$ in Eq. (8). In other words, although the SNR of the OCDM signal is compensated with a single iteration of IB-DFE, there are still decision errors because of, for example, noise and decision errors in the previous iteration. Similar to Fig. 6, the measured constellation diagrams of the received signal at an OSNR = 40 dB are shown in Fig. 10. It can be seen that once the IB-DFE is applied, the diagram becomes clustered since the fading effect is compensated. The scattered symbols (errors) in the diagram are gradually reduced with more iterations as the IB-DFE corrects the errors iteration by iteration.

D. Comparison with Adaptive DMT-OFDM System

In the above subsection, we considered an open-loop system, and the transmitter has no knowledge of the CSI. The proposed IB-DFE receiver recovers the corrupted information in the vicinity of the frequency notches, and significantly improves the performance of OCDM signal. Research work demonstrates that in a close-loop system, if the transmitter has knowledge of CSI, system capacity can be improved by adaptively modulating the information according to the CSI at the transmitter end, such as pre-compensation or adaptive modulation [26-29].

In this subsection, we provide experimental comparison with adaptive modulated DMT system based on the acquired CSI. It should be noted that we still assume that the proposed OCDM is open-loop system, without any pre-compensation at the transmitter. In the adaptive modulated DMT, based on the measured CFR, the first 250 subcarriers were 64-QAM, and the following 200 and 140 subcarriers were 32- and 16-QAM modulated. As the SNR dropped dramatically in the high frequency region, the remaining 10 and 30 subcarriers were in 8- and 4-QAM modulated, respectively. The data rate thus increased to 37.9 Gbit/s. In contrast, there was no change in the proposed OCDM system, except that we pushed the data rate to 37.9 Gbit/s by simply using 32-QAM for a fair comparison in terms of data rate. However, in terms of system complexity, the proposed OCDM system is much simpler as there is no feedback link and no extra complexity to coordinate the transmitter and receiver. For both systems, the rest of the setups are the same as the previous subsection.

The measured BER performance is provided in Fig. 11. It can be seen that for the DMT system, adaptive modulation not only increases the data rate but also slightly improves the BER performance. The received constellation diagrams of the 16-, 32, and 64-QAM at an OSNR = 40 dB are provided in the insets in Fig. 11. The adaptive modulated DMT signal can attain a BER of ~2×10^{-4} at an OSNR = 48 dB. In contrast, degradation occurs in the OCDM system as the higher modulation level is susceptible to noise and interference. However, if IB-DFE is applied, the BER is improved to 3×10^{-5}. The proposed OCDM system with 4 iterations needs ~5-dB OSNR less than the adaptive DMT-OFDM to achieve a BER = 2×10^{-4}. To emphasize, in the experiment, we still assume that the OCDM transmitter has no knowledge of the CSI.

V. Discussions

In Section III and IV, simulations and experiments were realized to investigate the proposed OCDM system with IB-DFE. The proposed IB-DFE receiver can improve the performance by compensating the fading effect caused by CD, for example. Only the receiver needs the CSI by channel estimation, and the transmitter remains unchanged. It is shown that in an open-loop system, the proposed system attains superior performance compared to a conventional OFDM system.

Further comparison with an adaptive bit-loading modulated OFDM is provided. With the knowledge of CSI available at the transmitter, it is shown that the adaptive OFDM has better performance than the OCDM without IB-DFE by allocating lower modulation levels to the subcarriers in the frequency notches. If IB-DFE is applied, an open-loop OCDM system again outperforms the adaptive OFDM. Moreover, the proposed OCDM is much simpler than the adaptive OFDM scheme as adaptive

bit/power loading algorithm requires not only a feedback control channel, but also extra complexity and system overhead to coordinate the transmitter and receiver. In practical optical systems, the cost of deploying a feedback link may not be acceptable, particularly in cost-sensitive short-reach systems.

Nonetheless, adaptive modulation, such as pre-compensation can be applied to the OCDM system if the transmitter has the knowledge of CSI. In particular, adaptive pre-compensation can be combined with the IB-DFE algorithm to further extend the reach and capacity of the proposed system. In contrast, IB-DFE cannot be applied to the OFDM system. In the OFDM based system, information is modulated onto the narrowband subcarriers in the frequency domain. There is no ISI for the subcarriers, and thus the IB-DFE algorithm cannot cancel the ISI or equivalently compensate the fading effect in the frequency domain.

In addition, in this paper, we employed a 50-km fiber for a proof-of-concept experiment in the L-band, in which the first frequency notch occurs at 8.5 GHz. Due to this limitation, in this paper, we experimentally demonstrated OCDM with IB-DFE at 30.3 Gbit/s for 16-QAM and 37.9 Gbit for 32-QAM. However, the data rates can be flexibly scaled by moving to wavelength bands where the CD is lower. For example, for the next-generation Terabit Ethernet, 100G per lane is preferred over 10 km in the O-band. In this case, the frequency notches occurs above 50 GHz, and a data rate over 112 Gbit/s can be easily realized [14].

VI. Conclusion

In this paper, we proposed an IM/DD-OCDM with IB-DFE to effectively compensate the fading effect in the IM/DD based system. The model of the proposed system is formulated mathematically and a simplified IB-DFE algorithm is derived based on the property of DFnT. Both simulation and experiment were carried out to holistically study the proposed system. A 30.3-Gbit/s IM/DD-OCDM signal transmission was experimentally demonstrated over 50 km of fiber. The results show that the proposed IM/DD-OCDM system has superior performance to OFDM even without the IB-DFE. If the IB-DFE is applied, the performance of the proposed system is further improved. In the experiment, it is shown that the required OSNR to achieve a BER = 3×10^{-5} is reduced by 7 dB with 4 iterations. These advantages make the proposed system an attractive solution for future high-speed short-reach systems, such as PON and datacenter interconnects.

References

[1] P. J. Winzer and R. J. Essiambre, "Advanced optical modulation formats," *Proc. IEEE,* vol. 94, no. 5, pp. 952–985, May 2006.

[2] J. C. Rasmussen and T. Drenski, "DSP for short reach optical links," in *Proc. ECOC*, Gothenburg, Sweden, 17-21 Sept. 2017, pp. 1–3.

[3] K. Zhong *et al.*, "Digital signal processing for short-reach optical communications: A review of current technologies and future trends," *J. Lightw. Technol.,* vol. 36, no. 2, pp. 377–400, Jan. 2018.

[4] X. Ouyang and J. Zhao, "Orthogonal chirp division multiplexing," *IEEE Trans. Commun.,* vol. 64, no. 9, pp. 3946–3957, Jul. 2016.

[5] — —, "Orthogonal chirp division multiplexing for coherent optical fiber communications," *J. Lightw. Technol.,* vol. 34, no. 18, pp. 4376–4386, Aug. 2016.

[6] X. Ouyang *et al.*, "Chirp spread spectrum toward the Nyquist signaling rate — Orthogonality condition and applications," *IEEE Signal Process. Lett.,* vol. 24, no. 10, pp. 1488–1492, Aug. 2017.

[7] W. Shieh *et al.*, "Coherent optical OFDM: theory and design," *Opt. Express,* vol. 16, no. 2, pp. 841–859, Jan. 2008.

[8] J. Armstrong, "OFDM for optical communications," *J. Lightw. Technol.,* vol. 27, no. 3, pp. 189–204, Jan.–Feb. 2009.

[9] J. Lee *et al.*, "Discrete multi-tone transmission for short-reach optical connections," in *Proc. OFC*, Anaheim, CA, USA, 20-24 Mar. 2016, p. Th1G.1.

[10] G. J. Meslener, "Chromatic dispersion induced distortion of modulated monochromatic light employing direct detection," *IEEE J. Quantum Electron.,* vol. 20, no. 10, pp. 1208–1216, Oct. 1984.

[11] J. C. Rasmussen *et al.*, "Digital signal processing for short reach optical links," in *Proc. ECOC*, Cannes, France, 21-25 Sept. 2014, p. Tu.1.3.3.

[12] R. Urata *et al.*, "Datacenter interconnect and networking: from evolution to holistic revolution," in *Proc. OFC*, Los Angeles, CA, USA, 19-23 Mar. 2017, p. W3G.1.

[13] V. Houtsma *et al.*, "Recent progress on standardization of next-generation 25, 50, and 100G EPON," *J. Lightw. Technol.,* vol. 35, no. 6, pp. 1228–1234, Mar. 2017.

[14] X. Ouyang *et al.*, "Experimental demonstration of 112 Gbit/s orthogonal chirp-division multiplexing based on digital up-conversion for IM/DD systems with improved resilience to system impairments," in *Proc. ECOC*, Rome, Italy, 23-27 Sept. 2018, pp. 1-3.

[15] X. Ouyang *et al.*, "Iterative block decision feedback equalization for IM/DD-OCDM system to mitigate CD-induced fading," in *Proc. CLEO*, San Jose, CA, USA, 5-10 May 2019, p. SM3G.5.

[16] X. Ouyang *et al.*, "Discrete Fresnel transform and its circular convolution property," *arXiv.org,* vol. arXiv:1510.00574, 2015.

[17] F. Gori, "Why is the Fresnel transform so little known?," in *Current Trends in Optics*, J. C. Dainty, Ed., ed: Academic Press, 1994, pp. 139-148.

[18] G. H. Smith *et al.*, "Overcoming chromatic-dispersion effects in fiber-wireless systems incorporating external modulators," *IEEE Trans. Microw. Theory Techn.,* vol. 45, no. 8, pp. 1410-1415, 1997.

[19] D. Falconer *et al.*, "Frequency domain equalization for single-carrier broadband wireless systems," *IEEE Commun. Mag.,* vol. 40, no. 4, pp. 58-66, Apr. 2002.

[20] N. Benvenuto and S. Tomasin, "Iterative design and detection of a DFE in the frequency domain," *IEEE Trans. Commun.,* vol. 53, no. 11, pp. 1867-1875, Nov. 2005.

[21] N. Benvenuto *et al.*, "Single carrier modulation with nonlinear frequency domain equalization: An idea whose time has come — Again," *Proc. IEEE,* vol. 98, no. 1, pp. 69-96, Jan. 2010.

[22] J. Wu and Y. R. Zheng, "Low complexity soft-input soft-output block decision feedback equalization," *IEEE J. Sel. Areas Commun.,* vol. 26, no. 2, pp. 281-289, Feb. 2008.

[23] X. Liu and F. Buchali, "Intra-symbol frequency-domain averaging based channel estimation for coherent optical OFDM," *Opt. Express,* vol. 16, no. 26, pp. 21944-21957, Dec. 2008.

[24] X. Ouyang *et al.*, "Unbiased channel estimation based on the discrete Fresnel transform for CO-OFDM systems," *IEEE Photon. Technol. Lett.,* vol. 29, no. 8, pp. 691-694, Apr. 2017.

[25] X. Ouyang *et al.*, "Robust channel estimation for coherent optical orthogonal chirp-division multiplexing with pulse compression and noise rejection," *J. Lightw. Technol.,* vol. 36, no. 23, pp. 5600-5610, Dec. 2018.

[26] A. J. Goldsmith and C. Soon-Ghee, "Variable-rate variable-power MQAM for fading channels," *IEEE Trans. Commun.,* vol. 45, no. 10, pp. 1218-1230, Oct. 1997.

[27] T. Keller and L. Hanzo, "Adaptive multicarrier modulation: a convenient framework for time-frequency processing in wireless communications," *Proc. IEEE,* vol. 88, no. 5, pp. 611-640, May 2000.

[28] E. Giacoumidis *et al.*, "Adaptive loading algorithms for IMDD optical OFDM PON systems using directly modulated lasers," *J. Opt. Commun. Netw.,* vol. 4, no. 10, pp. 769-778, Oct. 2012.

[29] L. Zhang *et al.*, "Beyond 200-Gb/s DMT transmission over 2-km SMF based on a low-cost architecture with single-wavelength, single-DAC/ADC and single-PD," in *Proc. ECOC*, Rome, Italy, 23-27 Sept. 2018, pp. 1-3.

Xing Ouyang (M'09) received his M.Sc. degree in Information Science and Engineering from Dalian Polytechnic University, China in 2013, and a PhD in Electrical and Electronic Engineering from Tyndall National Institute, University College Cork, Ireland in 2017.

During his PhD, he was in the Photonic Systems Group, Tyndall National Institute, engaged in advanced digital signal processing technology for next-generation fiber-optic communication. In 2016, he was with Nanyang Technological University, Singapore, involved in the "Car-to-Car WiFi: Multi-Hop Video Streaming" project. He is now a researcher in the Photonic Systems Group, Tyndall National Institute, Cork, Ireland. His research topics include advanced DSP techniques, such as modulation formats, OFDM, and channel equalization, and their applications in both fiber-optic and radio-frequency systems.

Giuseppe Talli (S'01–M'03) received the Laurea degree in electronic engineering from the University of Padova, Padova, Italy, in 2000 and the Ph.D. degree in electronic engineering from the University of Essex, Essex, U.K., in 2003, for work on the effects of the amplified spontaneous emission in semiconductor optical amplifiers and their gain dynamics.

Since 2004, 2004 to 2008 he has been with the Photonic Systems Group at the Tyndall National Institute, University College Cork, Ireland, as a post-doctoral scientist. From 2008 to 2012 has been with Intune Networks, Dublin, working on design and implementation of photonic subsystems for optical burst switching in metro networks. Since July 2012 he has rejoined the Tyndall National Institute as staff research scientist, working in the area of next generation optical access networks including metro-scale passive optical network (PON) architectures and burst-mode subsystems.

Mark Power

Paul D. Townsend (M'04) received the B.Sc. degree in physics from the University of East Anglia, Norwich, U.K., in 1983 and the Ph.D. degree in physics from the University of Cambridge, Cambridge, U.K., in 1987.

From 1987 to 1990, he held a joint position with St. John's College, Cambridge, and with Bellcore, Red Bank, NJ, and in 1990, he joined British Telecom Laboratories, Ipswich, U.K., where he worked on various aspects of quantum optics and optical communications including quantum cryptography. In 2000, he joined the Corning Research Centre, Ipswich, where he was a Project Manager for access network applications research. Since 2003, he has been with the Tyndall National Institute and the Department of Physics, University College Cork, in Ireland, where he is a Research Professor. He is currently Head of Photonics at Tyndall and Director of the Irish Photonic Integration Centre (IPIC). His research interests include optical and quantum communications. Prof.. Townsend is a Fellow of the Institute of Physics (U.K. and Ireland)